Vortex-chain phases in layered superconductors

A. E. Koshelev
Materials Science Division, Argonne National Laboratory, Argonne, Illinois 60439, USA
(Received 3 January 2005; published 19 May 2005)

Layered superconductors in tilted magnetic field have a very rich spectrum of vortex lattice configurations. In the presence of in-plane magnetic field, a small *c*-axis field penetrates in the form of isolated vortex chains. The structure of a single chain is mainly determined by the ratio of the London (λ) and Josephson (λ_J) lengths, $\alpha=\lambda/\lambda_J$. At large α the chain is composed of tilted vortices (tilted chains) and at small α it consists of a crossing array of Josephson vortices and pancake stacks (crossing chains). We studied the chain structures at intermediate α's and found two types of behavior. (i) In the range $0.4\lesssim\alpha\lesssim0.5$ a *c*-axis field first penetrates in the form of pancake-stack chains located on Josephson vortices. Due to attractive coupling between deformed stacks, their density jumps from zero to a finite value. With further increase of the *c*-axis field the chain structure smoothly evolves into modulated tilted vortices and then transforms via a second-order phase transition into the tilted straight vortices. (ii) In the range $0.5\lesssim\alpha\lesssim0.65$ a *c*-axis field first penetrates in the form of kinks creating kinked tilted vortices. With increasing the *c*-axis field this structure is replaced via a first-order phase transition by the strongly deformed crossing chain. This transition is accompanied by a large jump of pancake density. Further evolution of the chain structure is similar to the higher anisotropy scenario: it smoothly transforms back into the tilted straight vortices.

DOI: 10.1103/PhysRevB.71.174507 PACS number(s): 74.25.Qt, 74.25.Op, 74.20.De

I. INTRODUCTION

Layered superconductors have an amazingly rich phase diagram in tilted magnetic field. In the presence of the in-plane field, pancake vortices generated by the *c*-axis field[1,2] can form a very large number of different lattice configurations. Possible structures include the kinked lattice,[3–6] tilted vortex chains,[7] and crossing lattices composed of sublattices of Josephson vortices (JVs) and pancake-vortex stacks.[4,8] In addition to homogeneous lattices, phase-separated states may also exist such as dense pancake-stack chains sitting on JVs and dilute lattice in between[8–11] or coexisting lattices with different orientations.[12] Even though considerable progress in this field has been made in the last decade, the satisfactory understanding of the phase diagram has not been achieved yet. All these phases probably do realize in different materials and experimental conditions. However, finding ground states in tilted field occurs to be a challenging theoretical task and it is even more difficult to prove experimentally that a particular lattice configuration does realize somewhere in the phase diagram.

The main source of richness of lattice structures in tilted field is the existence of two very different kinds of interactions between pancake vortices in different layers: magnetic and Josephson interactions. The key parameter, which determines the relative strength of these two interactions and plays a major role in selecting the lattice structures, is the ratio of the two fundamental lengths, the in-plane London penetration depth, $\lambda\equiv\lambda_{ab}$, and Josephson length $\lambda_J=\gamma s$, with γ being the anisotropy parameter and s being the interlayer spacing, $\alpha=\lambda/\lambda_J$. One can distinguish two limiting cases which we refer to as "extremely anisotropic" case, $\alpha<0.4$, and "moderately anisotropic" case $\alpha>0.7$. Note that in our terminology even "moderately anisotropic" superconductors may have very large anisotropy factor, $\gamma\gg1$. Among known atomically layered superconductors, only $Bi_2Sr_2CaCu_2O_x$ (BSCCO) and related compounds may belong to the "extremely anisotropic" family. Even in this compound the parameter α is not smaller than ~0.25 and increases with temperature so that BSCCO typically becomes "moderately anisotropic" in the vicinity of transition temperature.

In a wide range of the in-plane fields (10–200 G) and at very small *c*-axis fields (up to 1–2 G) the pancake stacks in layered superconductors within a wide range of anisotropies are arranged in chains, see Fig. 1. An isolated chain is a two-dimensional array of pancake vortices oriented perpendicular to the layers. At somewhat higher *c*-axis fields the chains are surrounded by the stripes of regular vortex lattice.[9,10] The internal structure of an isolated chain depends on the ratio α and it is relatively simple in two limiting cases. At large α the chain is composed of tilted pancake stacks (tilted chain, right column in Fig. 1) and at small α it consists of crossing array of Josephson vortices and pancake stacks (crossing chains, left column in Fig. 1). A very nontrivial and intriguing problem is how one structure transforms into another in the region of intermediate α. We address this problem in this paper. We analytically and numerically computed

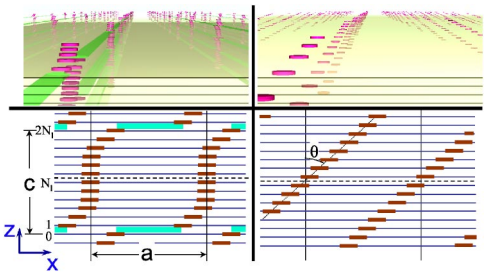

FIG. 1. (Color online) Crossing (left) and tilted (right) vortex chains. Upper pictures show three-dimensional views and lower pictures show the structures of isolated chains.

ground-state configurations in the isolated vortex chain and found a surprisingly rich behavior. We found two types of phase transitions. The first phase transition typically takes place for the intermediate separations between pancake stacks a, $a=(1-2)\lambda_J$, and rather wide range of the ratio α, $0.4\lesssim\alpha\lesssim 0.65$. For these α's the ground state is given by the crossing chain in a wide range of the pancake separations a. However, due to attractive coupling between deformed pancake stacks,[13] the equilibrium separation cannot exceed some maximum value, which depends on the in-plane field and α and it is typically of the order of several λ_J. With decreasing the pancake separation a, the crossing chain becomes strongly deformed and smoothly transforms into the modulated tilted vortices which then transform via a second-order phase transition into the tilted straight vortices. We calculated analytically the energies of two limiting chain configurations and checked that numerics reproduces them. Comparing these energies, we locate the transitional region in the phase space, where strongly deformed chains are realized.

Another phase transition is realized at very small densities of pancake vortices and only when α exceeds a certain critical value ≈ 0.5 (exact criterion depends on the in-plane magnetic field). In this case a small c-axis field penetrates in the form of kinks. The kinked vortex lines forming tilted chains are composed of pieces of Josephson vortices separated by kinks.[3–5] If the kink energy is only slightly smaller than the energy per pancake in a straight pancake stack then at very small concentration of kinks, typically at $a\approx(20-30)\lambda_J$, the kinked chains are replaced with strongly deformed crossing chains via a first-order phase transition. Due to the opposite signs of interactions (kinks repel and deformed pancake stacks attract each other), this transition is accompanied by a very large jump in the pancake density. With further decrease of pancake separation the chain smoothly transforms back to the tilted chain as it was described in the previous paragraph.

Based on numerical exploration of the chain configurations, we construct the chain phase diagrams for different ratios α. As follows from the earlier description, there are two types of phase diagrams in the region of intermediate α's.

• In the range $0.4\lesssim\alpha\lesssim 0.5$ a small c-axis field first penetrates in the form of pancake-stack chains located on Josephson vortices. Due to attractive coupling between deformed stacks, their density jumps from zero to a finite value. With further increase of the c-axis field the chain structure first evolves into the modulated tilted vortices, which then transforms via a second-order phase transition, into the tilted straight vortices.

• In the range $0.5\lesssim\alpha\lesssim 0.65$ a small c-axis field first penetrates in the form of kinks creating kinked tilted vortices. With increasing the c-axis field this structure is replaced via a first-order phase transition by the chain of pancake stacks, which are typically strongly deformed. This transition is accompanied by a large jump of pancake density. Further evolution of the chain structure is identical to the smaller α scenario: the structure first transforms into modulated tilted vortices and then, via a second-order phase transition, into tilted straight vortices.

Note that the exact transition between the two types of behavior depends also on the in-plane field. As interaction with the Josephson vortices reduces the energy of the pancake stacks, the larger in-plane field favors the first scenario.

Using numerical code developed for studying the chain structures, we also investigated stability of an isolated crossing configuration of the Josephson vortex and pancake stack. We found that the crossing configuration becomes unstable at $\alpha\approx 0.69$. Above this value the magnetic coupling is not capable to maintain stable configuration and the Josephson vortex tears the stack apart. Nevertheless, the obtained stability range occurs to be significantly broader than it was estimated from simple considerations in Ref. 21. The reason is that the strongly deformed crossing configuration significantly modifies the Josephson vortex which reduces forces pulling pancakes apart. We found that the crossing energy increases smoothly up to instability point. Perturbative calculation[8] gives accurate results for the crossing configuration and its energy up to $\alpha\approx 0.35$.

Recently, the vortex chains in BSCCO at small concentrations of pancakes have been studied by the scanning Hall probe microscopy by Grigorenko *et al.*[14] They observed that at very small concentration of the pancakes the chains are magnetically homogeneous and separate pancake stacks are not resolved. When the external field exceeds some critical value of the order of several oersted, crystallites of the pancake stacks are suddenly formed along the chain and the flux density in the crystallites approximately ten times higher then the flux density in the homogeneous chains. Our calculations provide consistent interpretation for these observations. The magnetically homogeneous chains are interpreted as kinked/tilted chains and formation of crystallites can be attributed to the low-density (kinked lines)-(crossing chains) first-order phase transition (such interpretation has been proposed by Dodgson[15]). The observed large density jump also comes out from the theory.

The evolution of the mixed chain+lattice state with increasing temperature has been studied recently by Lorentz microscopy.[16] It was observed that the pancake stacks located in chains smear along the chain direction above some field-dependent temperature while the pancake stacks outside chains still remain well defined. The continuous low-density phase transition from crossing to tilted chain found and discussed in this paper provides a very natural interpretation for this observation.

The paper is organized as follows. In Sec. II we review general expressions for the chain energy. In Sec. III we perform analytical calculations of the chain energy for the two limiting cases: crossing and tilted chain. In Sec. IV, comparing energies for the two limiting configurations, we estimate location of the transition region. In Sec. V we review attractive interaction between deformed pancake stacks located on Josephson vortices[13] and derive general formulas for determination of the maximum equilibrium separation between the pancake stacks and the boundaries of stability region with respect to density fluctuations. Section VI contains the main results of the paper on numerical exploration of the the phase diagram. After discussion of numerical implementation of the model, we explore stability of the isolated crossing configuration. In the next two subsections we consider two different phase transitions between the tilted and crossing chains and two types of phase diagrams which are real-

ized in the region of intermediate parameter α.

II. ENERGY FUNCTIONAL

Our calculations are based on the Lawrence-Doniach free-energy functional in the London approximation, which depends on the in-plane phases $\phi_n(\mathbf{r})$ and vector-potential $\mathbf{A}(\mathbf{r})$

$$F = \sum_n \int d^2\mathbf{r}\left\{\frac{J}{2}\left(\nabla_\perp \phi_n - \frac{2\pi}{\Phi_0}\mathbf{A}_\perp\right)^2 + E_J\left[1-\cos\left(\phi_{n+1}-\phi_n-\frac{2\pi s}{\Phi_0}A_z\right)\right]\right\} + \int d^3\mathbf{r}\frac{\mathbf{B}^2}{8\pi}, \tag{1}$$

where

$$J \equiv \frac{s\varepsilon_0}{\pi} \text{ and } E_J \equiv \frac{\varepsilon_0}{\pi s\gamma^2} \tag{2}$$

are the phase stiffness and the Josephson coupling energy with $\varepsilon_0 \equiv \Phi_0^2/(4\pi\lambda)^2$, $\lambda \equiv \lambda_{ab}$ and λ_c are the components of the London penetration depth, $\gamma = \lambda_c/\lambda_{ab}$ is the anisotropy factor, and s is the interlayer periodicity. The ratio of the two energy scales determines the most important length scale of the problem, the Josephson length, $\lambda_J = \gamma s = \sqrt{J/E_J}$. We use the London gauge, div $\mathbf{A}=0$. We mainly address the situation when magnetic $\mathbf{B}$ inside the superconductor is fixed. The c component of the field determines the concentration of the pancake vortices $n_v \equiv B_z/\Phi_0$ inside one layer. The in-plane phases ϕ_n have singularities at the positions of pancake vortices $\mathbf{R}_{n,i}$ inside the layers

$$[\nabla \times \nabla \phi_n]_z = 2\pi\sum_i \delta(\mathbf{r}-\mathbf{R}_{n,i}).$$

Logarithmic divergencies in the vicinity of pancake-vortex cores have to be cut at the coherence length ξ_{ab}. A useful approach for superconductors with weak Josephson coupling is to split the phase and vector-potential into the vortex and regular contributions, $\phi_n = \phi_{vn} + \phi_{rn}$ and $\mathbf{A} = \mathbf{A}_v + \mathbf{A}_r$. The vortex contributions minimize the energy for fixed positions of pancake vortices at $E_J = 0$ and give magnetic interaction energy for the pancake vortices. One can express this part of energy via the vortex coordinates $\mathbf{R}_{n,i}$. In general, the regular contributions may include phases and vector potentials of the Josephson vortices. The total energy naturally splits into the regular part F_r, the energy of magnetic interactions between pancakes F_M, and the Josephson energy F_J, which couples the regular and vortex degrees of freedom

$$F = F_r + F_M + F_J \tag{3}$$

with

$$F_r[\phi_{rn}, \mathbf{A}_r] = \sum_n \int d^2\mathbf{r}\frac{J}{2}\left(\nabla\phi_{rn} - \frac{2\pi}{\Phi_0}\mathbf{A}_{r\perp}\right)^2 + \int d^3\mathbf{r}\frac{\mathbf{B}_r^2}{8\pi}, \tag{4}$$

$$F_M[\mathbf{R}_{n,i}] = \frac{1}{2}\sum_{n,m,i,j} U_M(\mathbf{R}_{n,i} - \mathbf{R}_{m,j}, n-m), \tag{5}$$

$$F_J[\phi_{rn}, \mathbf{A}_r, \mathbf{R}_{n,i}] = \sum_n \int d^2\mathbf{r} E_J\left[1-\cos\left(\nabla_n\phi_n - \frac{2\pi s}{\Phi_0}A_z\right)\right], \tag{6}$$

where the discrete gradient $\nabla_n\phi_n$ is defined as $\nabla_n\phi_n \equiv \phi_{n+1} - \phi_n$, and $U_M(\mathbf{R}, n)$ is the magnetic interaction between pancakes[1]

$$U_M(\mathbf{R}, n) \approx 2\pi J\left[\ln\frac{L}{R}\left[\delta_n - \frac{s}{2\lambda}\exp\left(-\frac{s|n|}{\lambda}\right)\right] + \frac{s}{4\lambda}u\left(\frac{r}{\lambda}, \frac{s|n|}{\lambda}\right)\right], \tag{7}$$

$$u(r,z) \equiv \exp(-z)E_1(r-z) + \exp(z)E_1(r+z),$$

where $E_1(u) = \int_u^\infty (\exp(-v)/v)dv$ is the integral exponent [$E_1(u) \approx -\gamma_E - \ln u + u$ at $u \ll 1$ with $\gamma_E \approx 0.5772$ being the Euler constant], $r \equiv \sqrt{R^2 + (ns)^2}$, and L is a cutoff length. The regular and vortex degrees of freedoms are coupled only via the Josephson energy in which ϕ_n is the total phase composed of vortex and regular contributions.

The discrete layer structure has strongest influence on the cores of tilted and Josephson vortices. Interaction contributions to the total energy usually can be computed within continuous approximation which describes the layered superconductor as a three-dimensional anisotropic material. This approximation amounts to replacement of summation in the layer index n in Eqs. (4)–(6) with integration in the continuous variable $z = ns$ and expansion of cosine in Eq. (6). In the continuous approximation one can derive a very useful general result for the energy (1) (see Ref. 17)

$$F = \frac{\Phi_0^2}{8\pi}\int \frac{d^3\mathbf{k}}{(2\pi)^3}\frac{(1+\lambda_c^2k^2)|S_z|^2 + (1+\lambda^2k^2)|S_\parallel|^2}{(1+\lambda^2k^2)(1+\lambda^2k_z^2+\lambda_c^2k_\parallel^2)} \tag{8}$$

in terms of vorticity $\mathbf{S}(\mathbf{r})$ of parametrically defined vortex lines $\mathbf{R}_i(X)$

$$\mathbf{S}(\mathbf{r}) = \sum_j \int dX \frac{d\mathbf{R}_i}{dX}\delta[\mathbf{r} - \mathbf{R}_i(X)]$$

whose Fourier transform is

$$\mathbf{S}(\mathbf{k}) = \sum_j \int dX \frac{d\mathbf{R}_j}{dX}\exp[i\mathbf{k}\mathbf{R}_j(\mathbf{X})].$$

As we will use this formula only for evaluation of interaction energies between vortex lines, we have to subtract from it the logarithmically diverging single-vortex terms.

In this paper we focus on the structure of an isolated vortex chain with period a in x direction and period $c = Ns$ in z direction corresponding to the tilting angle θ of vortices with respect to the c axis with $\nu \equiv \tan\theta = a/c$ (see Fig. 1). The vertical period is fixed by the in-plane field B_x, $c \approx \sqrt{2\Phi_0/(\sqrt{3}\gamma B_x)}$. For BSCCO $\gamma \sim 500$ and this period is approximately equal to 20 layers at $B_x \approx 50$ G. We consider

the case $c \ll \lambda$ and in-plane distances much smaller than λ_c. For this particular problem the general energy given by Eqs. (3)–(6) can be significantly simplified using several approximations: (i) we can neglect screening of regular phase and z-axis vector potential; (ii) we consider only one-dimensional displacements of pancake rows along the chain, $\mathbf{R}_{n,i}=(ai+u_n,0,ns)$; (iii) we subtract the energy of straight pancake stacks, $(B_x/\Phi_0)\varepsilon_{\rm PS}$ with $\varepsilon_{\rm PS}\approx\varepsilon_0(\ln\kappa+0.5)$, allowing us to eliminate logarithmically diverging pancake-core contributions; and (iv) we drop the trivial magnetic energy term $B_x^2/8\pi$ which plays no role in selection between different chain phases. We will use the chain energy per unit area, $E\equiv c_y[F/V-B_x^2/(8\pi)-(B_z/\Phi_0)\varepsilon_{\rm PS}]$ with V being the total system volume. With the introduced simplifications this energy can be represented as

$$E=\frac{1}{sN}\sum_{n=1}^{N}\int_0^a\frac{dx}{a}\int_{-c_y/2}^{c_y/2}dy\left(\frac{J}{2}(\nabla\phi_{r,n})^2+E_J\left\{1-\cos\left[\nabla_n(\phi_{r,n}+\phi_{v,n})-\frac{2\pi s}{\Phi_0}B_x y\right]\right\}\right)+\frac{1}{2sL_z}\sum_{n\neq m}U_{Mr}(u_n-u_m,n-m), \tag{9}$$

where $\phi_{v,n}(\mathbf{r})$ is the vortex-phase variation induced by displacement of pancake rows, u_n, from the ideally aligned positions

$$\varphi_{v,n}(x,y;u_n)=\arctan\frac{\tan(\pi(x+u_n)/a)}{\tanh(\pi y/a)}-\arctan\frac{\tan(\pi x/a)}{\tanh(\pi y/a)},$$

$U_{Mr}(u_n-u_m,n-m)$ is the interaction energy between the pancake rows per unit length, computed with respect to straight stacks

$$U_{Mr}(u,n)\equiv\frac{1}{a}\sum_m[U_M(ma+u,n)-U_M(ma,n)], \tag{10}$$

$c_y=\Phi_0/cB_x\gg c$ is the in-plane distance between chains, and L_z is the total system length in z direction.

The energy (9) contains a long-range suppression of the Josephson energy accumulated from distances $c\ll y\ll c_y$, that is identical in all chain phases and it is convenient to separate this term too. The averaged z-axis phase gradient induced by the Josephson vortex lattice is given by

$$\overline{\nabla_n\phi_n}-\frac{2\pi s}{\Phi_0}B_x y=\frac{\pi}{N}-\frac{2\pi y}{Nc_y}.$$

Evaluating integral

$$\int_{-c_y/2}^{c_y/2}dy\left[1-\cos\left(\nabla_n\overline{\phi_n}-\frac{2\pi s}{\Phi_0}B_x y\right)\right]\approx\frac{\pi^2 c_y}{6N^2},$$

we obtain the long-range Josephson energy, $E_{\rm J\text{-}LR}$,

$$E_{\rm J\text{-}LR}=E_J\frac{\pi^2 c_y}{6sN^2} \tag{11}$$

We will define the local energy, E_{loc}, sensitive to the chain structure as

$$E_{loc}\equiv E-E_{\rm J\text{-}LR}. \tag{12}$$

This part of energy weakly depends on c_y and does not diverge for $c_y\to\infty$. The result (11) is valid for chains separated by distance c_y smaller than λ_c. Similar calculation can be made for an isolated chain separated from other chains by distance larger than λ_c. In this situation the integral over y converges on distance λ_c instead of c_y leading to result $E_{\rm J\text{-}LR}=E_J\pi\lambda_c/sN^2$. We will use this result in the analytical calculations of the isolated chain energy.

In calculation of magnetic coupling energy one has to take into account periodic conditions for pancake displacements, $u_{n+N}=u_n$. In addition, if one selects z axis origin at the center of the Josephson vortex then symmetry also requires $u_{-n}=-u_n$. Ground state of the vortex chain is determined by the minimum of energy (9) with respect to pancake displacements and regular phase distribution. Two simple limiting cases in Fig. 1 correspond to (i) $u_n\ll a$ for the crossing-chain configuration and (ii) $u_n=-a[1-(n-1/2)/N_l]/2$ for the tilted-chain configuration.

III. ANALYTICAL CALCULATIONS OF CHAIN ENERGIES

In this section we compute energy of an isolated vortex chain with period a in x direction and period $c=Ns\ll\lambda$ in z direction. In general, there are two approaches to compute energies of vortex configurations. Using distribution of phase and vector potential, the total energy can be obtained directly from the Lawrence-Doniach functional by integration of the local energy. This approach is always used in numerical computations. Analytically, it is more convenient to calculate the total energy by summing up energy of isolated vortices and vortex interactions. Analytic estimates for energy contributions are possible in two limiting cases of weakly deformed crossing chain and chain consisting of tilted vortices (see Fig. 1). Comparison of these energies gives an approximate range of parameters where one of these competing configurations is energetically preferable. In contrast to the numerical part, we consider isolated chain separated from other chains by distance $c_y\gg\lambda_c$. For comparison with numerical calculations, it will be necessary to extract the local part of energy which is not sensitive to the long-range behavior.

A. Crossing chains

Energy of crossing-lattices chain per unit area is given by sum of pancake stack (E_{PS}), Josephson vortex (E_{JV}) and crossing energies ($E_\times$) terms

$$E_{CL}=E_{PS}+E_{JV}+E_\times. \tag{13}$$

Both pancake and JV terms are composed of single-vortex and interaction contribution, $E_{PS}=E_{PS}^s+E_{PS}^i$, $E_{JV}=E_{JV}^s+E_{JV}^i$.

We start with evaluating pancake-stack energies. Contribution from energies of individual stacks to the energy per unit length is given by

$$E_{PS}^s=\frac{\varepsilon_0}{a}\left(\ln\frac{\lambda}{\xi}+C_v\right), \tag{14}$$

where $C_v\approx0.497$ within the Ginzburg-Landau theory. Using vorticity of the pancake-vortex chain, $S_z(\mathbf{r})=\Sigma_j\delta(y)\delta(x-ja)$

corresponding to $S_z(\mathbf{k})=\delta(k_z)\Sigma_j \exp(ik_x ja)$, we derive from general formula (8) the pancake-stacks interaction energy

$$E^i_{PS}=\frac{\Phi_0^2}{8\pi a}\int \frac{dk_x dk_y}{(2\pi)^2}\sum_{j\neq 0}\frac{\exp(ik_x ja)}{1+\lambda^2 k^2}. \tag{15}$$

Using relation $\Sigma_j \exp(ik_x ja)=(1/a)\Sigma_m \delta[k_x-(2\pi m/a)]$ and integrating over k_y, we obtain

$$E^i_{PS}=\frac{\Phi_0^2}{16\pi a^2\lambda}\sum_{m=-\infty}^{\infty}\frac{1}{\sqrt{1+(2\pi\lambda m/a)^2}} - \frac{\Phi_0^2}{16\pi a\lambda}\int\frac{dk}{2\pi}\frac{1}{\sqrt{1+\lambda^2k^2}}.$$

For comparison with the energy of tilted chain, it will be convenient to represent this energy in the form

$$E^i_{PS}=\frac{\varepsilon_0}{a}\left[\frac{\pi\lambda}{a}-\ln\frac{4\pi\lambda}{a}+\gamma_E-U\left(\frac{a}{2\pi\lambda}\right)\right] \tag{16}$$

with

$$U(x)=\sum_{m=1}^{\infty}\left(\frac{1}{m}-\frac{1}{\sqrt{m^2+x^2}}\right)=\begin{cases}\zeta(3)x^2/2, x\lesssim 0.5\\ \dfrac{1}{2x}-\ln\dfrac{2}{x}+\gamma_E, x\gtrsim 1\end{cases},$$

and $\zeta(3)\equiv\Sigma_{m=1}^{\infty}(1/m^3)\approx 1.202$.

Single-vortex JV energy is given by[6,18]

$$E^s_{JV}=\frac{\varepsilon_0}{\gamma c}\left(\ln\frac{\lambda}{s}+1.54\right).$$

The JV interaction energy can be evaluated in the same way as the pancake-stack interaction energy (16) and in the limit $c\ll\lambda$ it is given by

$$E^i_{JV}\approx\frac{\varepsilon_0}{\gamma c}\left(\frac{\pi\lambda}{c}-\ln\frac{4\pi\lambda}{c}+\gamma_E\right).$$

Therefore, the total energy of the JV array, $E_{JV}=E^s_{JV}+E^i_{JV}$, can be written as

$$E_{JV}=\frac{\varepsilon_0}{\gamma c}\left(\frac{\pi\lambda}{c}+\ln\frac{c}{s}+C_{JV}\right) \tag{17}$$

with $C_{JV}=1.54-\ln 4\pi+\gamma_E\approx -0.41$. The fist term in this formula is the long-range Josephson energy, $E_{\text{J-LR}}$. This term is identical in all chain phases and does not determine selection between them. This formula is valid for an isolated chain and it is different from the long-range Josephson energy of the dense JV lattice, $c_y<\lambda_c$, given by Eq. (11). The difference amounts to a simple replacement $c_y\to\pi\lambda_c$. For comparison with simulations, we will use only the local part of energy which is obtained from the total energy by subtracting $E_{\text{J-LR}}$.

Using estimate for the crossing energy of Josephson vortex and pancake stack for $\alpha=\lambda/\gamma s\lesssim 0.4$[8,19]

$$\epsilon_\times=-\frac{8\alpha^2 s\varepsilon_0}{\ln(3.5/\alpha)}, \tag{18}$$

we obtain the contribution from the crossings into the energy per unit area

$$E_\times=\frac{\epsilon_\times}{ac}=-\frac{8\alpha^2\varepsilon_0}{\ln(3.5/\alpha)aN}. \tag{19}$$

Finally, combining results (14), (16), (17), and (19), we obtain the total energy of crossing chain

$$E_{CL}=E^s_{PS}+\frac{\varepsilon_0}{a}\left[\frac{\pi\lambda}{a}-\ln\frac{4\pi\lambda}{a}+\gamma_E-U\left(\frac{a}{2\pi\lambda}\right)+\frac{\pi\nu\lambda}{\gamma c}+\frac{\nu}{\gamma}(\ln N+C_{JV})-\frac{8\alpha^2}{\ln(3.5/\alpha)N}\right]. \tag{20}$$

Subtracting the pancake-stack and long-range Josephson energies, we obtain local energy, $E^{loc}_{CL}=E_{CL}-E_{PS}-\varepsilon_0\pi\lambda/\gamma c^2$

$$E^{loc}_{CL}=\frac{\varepsilon_0}{a}\left[\frac{\nu}{\gamma}(\ln N+C_{JV})-\frac{8\alpha^2}{\ln(3.5/\alpha)N}\right], \tag{21}$$

which we will use for comparison with numerical simulations.

B. Tilted chains

Energy of the tilted chain per unit area also can be decomposed into the single-vortex and interaction contributions

$$E_{TV}=E^s_{TV}+E^i_{TV}.$$

The first term can be estimated analytically only in two limiting cases $\tan\theta\ll\gamma$ and $\tan\theta>\gamma$, where the second case corresponds to kinked lines. For the interaction term we derive a general formula valid in both limits.

1. Energy of a single tilted line

(a) *Region* $\nu=\tan\theta<\gamma$. Energy difference between tilted and straight pancake stacks, $\varepsilon_{TV}-\varepsilon_{PS}$, determines tilt stiffness of pancake stack and contains magnetic and Josephson contribution, ε_M and ε_J. Magnetic part has been calculated by Clem[2]

$$\varepsilon_M=\varepsilon_0\ln\frac{\sqrt{1+\nu^2}+1}{2}.$$

The Josephson contribution to the tilt energy appears due to suppression of the Josephson interlayer coupling by mismatched pancakes. It can be evaluated as

$$\varepsilon_J=\varepsilon_0\frac{\nu^2}{2\gamma^2}\left(\ln\frac{\lambda_c}{s\nu}+C_J\right).$$

Numerical constant C_J can be computed exactly by matching logarithmic contributions coming from small and large distances[20] which gives $C_J=3\ln 2-\gamma_E$. Therefore, the single-vortex energy of the tilted chain is given by

$$E^s_{TV}=E^s_{PS}+\frac{\varepsilon_0}{a}\ln\frac{\sqrt{1+\nu^2}+1}{2}+\frac{\varepsilon_0}{a}\frac{\nu^2}{2\gamma^2}\left(\ln\frac{8\lambda_c}{s\nu}-\gamma_E\right). \tag{22}$$

Note that at not very large tilt angles, $\nu\lesssim 1$, the Josephson tilt energy is roughly γ^2 smaller than the magnetic tilt energy. Two terms become comparable at very large tilt angles, ν

$\sim\gamma$. In several papers the energy of a tilted line in *anisotropic three-dimensional* superconductor has been calculated.[7,17] This calculation is based on the London energy expression (8) employing elliptic cut off in k-integration $k_\parallel^2+k_z^2/\gamma^2<\xi_{ab}^{-2}$ to treat the vortex core. Strictly speaking, this approximation does not describe layered superconductors in which $\xi_c<s$. Nevertheless, in the region $\nu<\gamma$ it leads to the result similar to Eq. (22).

(b) *Region* $\nu=\tan\theta>\gamma$ (*kinked lines*). In the region $\tan\theta>\gamma$ the vortex lines have the kink structure, i.e., they are composed of kinks separated by JV pieces. Energy of such line per unit length is given by

$$\varepsilon_{\rm kl}=\varepsilon_{JV}+u_k/L+\varepsilon_{\rm ki}, \tag{23}$$

where $\varepsilon_{JV}=(\varepsilon_0/\gamma)(\ln(\lambda/s)+1.54)$ is the energy of Josephson vortex

$$u_k=s\varepsilon_0(\ln(\gamma s/\xi)+C_k) \tag{24}$$

is the kink energy,[4,6] $L=s\tan\theta$ is the separation between kinks, and $\varepsilon_{\rm ki}$ is the kink interaction energy. Numerical constant C_k in the kink energy has been estimated as -0.17 in Ref. 6. However more accurate numerical calculations of this paper give somewhat smaller value $C_k\approx-0.31$.

The interaction energy between neighboring kinks in the kinked line decays as $1/L^2$ up to $L<\lambda_c$ leading to relatively large interaction contribution to the total energy. The kink interaction energy is computed in details in Appendix A. In the region $L\ll\lambda_c$ the dominant interaction term in the energy of single line is given by

$$\varepsilon_{ki}=\frac{\gamma s^2\varepsilon_0}{2L^2}\left[\ln\left(\frac{\lambda_c}{L}\right)-\frac{3}{2}\right]. \tag{25}$$

Combining all contributions, we derive the following result for the single-vortex energy of a tilted chain, $E_{TV}^s=\varepsilon_{\rm kl}/c$, in the limit $\nu>\gamma$:

$$E_{TV}^s=E_{PS}^s+E_{JV}^s+\frac{\varepsilon_0}{a}\left\{\ln\frac{1}{\alpha}+C_{kv}+\frac{\gamma}{2\nu}\left[\ln\left(\frac{\lambda_c N}{a}\right)-\frac{3}{2}\right]\right\} \tag{26}$$

with $C_{kv}\equiv C_k-C_v\approx-0.81$. Note that the values of the numerical constants C_v and C_k depend on the core structure at small distances $r\sim\xi$ from its center, which evolves with temperature decrease. However, as this structure is exactly the same for the pancake vortex and kink, the difference C_k-C_v is not sensitive to behavior at small distances and remains the same down to low temperatures. Criterion $\ln(1/\alpha_c)+C_{kv}=0$ (corresponding to $\alpha_c\approx0.44$) separates the kink and pancake-stack penetration regimes of a small c-axis field for large N (somewhat larger value $\alpha_c\approx0.5$ has been given in Ref. 6). This critical value increases with decrease of N due to the crossing energies in the crossing chains. Penetration of the c-axis field in the presence on the in-plane field is frequently referred to as a lock-in transition.

2. Interaction energy of tilted vortices.

The interaction energy between tilted lines is not influenced much by the layered structure and it can be computed within the London approximation. In Appendix B we derive a general analytical formula for the interaction energy of tilted chain, E_{TV}^i

$$E_{TV}^i\approx\frac{\varepsilon_0}{a}\left\{\frac{\pi\nu\lambda}{\gamma c}+\frac{\pi\lambda}{a}-\frac{\sqrt{\nu^2+\gamma^2}}{\gamma}\left[\ln\left(\frac{4\pi\lambda\sqrt{\nu^2+\gamma^2}}{a}\right)-\gamma_E\right]+\ln\frac{\gamma+\sqrt{\nu^2+\gamma^2}}{1+\sqrt{1+\nu^2}}\right\}. \tag{27}$$

The first term in this formula represents again the long-range Josephson energy and it is identical to the first term in the energy of the Josephson chain (17). At large N this formula also gives the interaction energy of a kinked line for $\nu>\gamma$, because the kinked structure of tilted lines starts to influence their interaction only at very large tilting angle $\nu>N\gamma/2\pi$.[23] In the region $\nu\ll\gamma$ Eq. (27) simplifies as

$$E_{TV}^i\approx\frac{\varepsilon_0}{a}\left\{\frac{\pi\nu^2\lambda}{\gamma a}+\frac{\pi\lambda}{a}-\ln\left[\frac{2\pi\lambda(1+\sqrt{1+\nu^2})}{a}\right]+\gamma_E-\frac{\nu^2}{2\gamma^2}\left[\ln\left(\frac{4\pi\lambda_c}{a}\right)-\gamma_E+\frac{1}{2}\right]\right\}. \tag{28}$$

The last term represents change of the Josephson energy due to misalignment of pancakes in different stacks. Combining this term with the last term in Eq. (22), we obtain the total Josephson energy loss of tilted chain due to pancake misalignment

$$\delta E_{TV}=\frac{\varepsilon_0}{a}\frac{\nu^2}{2\gamma^2}\left(\ln\frac{2c}{\pi s}-\frac{1}{2}\right).$$

In the limit of kinked lines, $\nu\gg\gamma$, interaction energy reduces to

$$E_{TV}^i\approx\frac{\varepsilon_0}{a}\left\{\frac{\pi\nu^2\lambda}{\gamma a}+\frac{\pi\lambda}{a}-\frac{\nu}{\gamma}\left[\ln\left(\frac{4\pi\lambda}{c}\right)-\gamma_E\right]-\frac{\gamma}{2\nu}\left[\ln\left(\frac{4\pi\lambda}{c}\right)-1-\gamma_E\right]\right\}. \tag{29}$$

Note again that this result is valid until $\nu<N\gamma/2\pi$, where the kink structure of the tilted lines does not influence much interaction between them. The limit of larger ν corresponds to the regime of "kink walls" described in Ref. 6.

3. Total energy of tilted chains

Combining the interaction energy (28) with the energy of individual stacks (22), we obtain the total tilted-chain energy in the limits $c=Ns\ll\lambda$, $\nu\ll\gamma$

$$E_{TV}\approx E_{PS}^s+\frac{\varepsilon_0}{a}\left[\frac{\pi\nu\lambda}{\gamma c}+\frac{\pi\lambda}{a}-\ln\left(\frac{4\pi\lambda}{a}\right)+\gamma_E+\frac{\nu^2}{2\gamma^2}(\ln N-0.95)\right]. \tag{30}$$

This gives the following result for the local part of energy, $E_{TV}^{loc}\equiv E_{TV}-E_{PS}-\varepsilon_0\pi\lambda/\gamma c^2$

$$E_{TV}^{loc} = \frac{\varepsilon_0}{a}\left[U\left(\frac{a}{2\pi\lambda}\right) + \frac{\nu^2}{2\gamma^2}(\ln N - 0.95)\right]. \quad (31)$$

In this formula the first term represents the loss of the magnetic coupling energy in the tilted chain and the second term represents the Josephson energy loss.

In the region of kinked lines $\nu \gg \gamma$ (but $\nu \ll N\gamma/2\pi$), the total chain energy is obtained by combining Eqs. (26) and (29) giving

$$E_{TV} \approx E_{PS}^{s} + E_{JV} + \frac{\varepsilon_0}{a}\left\{ \ln\frac{\gamma s}{\lambda} + C_{kv} + \frac{\gamma}{2\nu}\left[\ln\left(\frac{\gamma N}{\nu}\right) + C_{\rm ki}\right]\right\} \quad (32)$$

with $C_{\rm ki} = -\ln 4\pi - 1/2 + \gamma_E \approx -2.454$.

IV. LOCATION OF TRANSITIONAL REGIONS IN THE PHASE SPACE

To find out whether the crossing or tilted chain is realized for given values of the parameters a, c, and α, we have to compare the energies of these states. Naively, one may think that intersection of the energy curves for the two states would correspond to a first-order phase transition between these states. However, as we will see from numerical simulations, in the region $\nu = \tan\theta < \gamma$ another scenario is realized. Typically, strongly deformed intermediate chain configurations develop in the transitional region providing a smooth transition between the two limiting configurations. Therefore, a simple energy comparison gives only an approximate location of the transitional region separating the two configurations.

In the region $\nu/\gamma = a/N\lambda_J \ll 1$ comparison of (20) and (30) gives the following criterion for the transitional region:

$$U\left(\frac{a}{2\pi\lambda}\right) - \frac{\nu}{\gamma}(\ln N - 0.41) + \frac{\nu^2}{2\gamma^2}(\ln N - 0.95) + \frac{8\alpha^2}{\ln(3.5/\alpha)N} = 0. \quad (33)$$

One can observe that the main competition takes place between the loss of the magnetic coupling energy for the tilted chain (first term) and strong suppression of the Josephson energy by JVs for the crossing chain (second term). Solution of this equation provides the boundary which can be written in the reduced form $a = \lambda_J N\, f(N,\alpha)$ with $f(N,\alpha) \ll 1$, i.e., the boundary shape in the plane a/λ_J-N depends only on the parameter α.

In region $1 < \nu/\gamma < N/2\pi$ and $a > 2\pi\lambda$ comparison of the energies (20) and (32) gives

$$\ln\frac{1}{\alpha} + C_{kv} + \frac{\gamma}{2\nu}\left[\ln\left(\frac{\gamma N}{\nu}\right) + C_{\rm ki}\right] + \frac{8\alpha^2}{\ln(3.5/\alpha)N} = 0. \quad (34)$$

This equation has a solution only in the kink penetration regime, $\ln(1/\alpha) + C_{kv} < 0$, near the transition between the two penetration regimes $|\ln(1/\alpha) + C_{kv}| \ll 1$ where the kink energy is only slightly smaller than the energy per pancake of a straight pancake-vortex stack. In contrast to Eq. (33), which gives only an approximate location of the broad transitional region, this equation indeed describes a very strong first-order phase transition.

V. ATTRACTION BETWEEN DEFORMED PANCAKE STACKS AND TILTED VORTICES: MAXIMUM EQUILIBRIUM SEPARATION

A peculiar property of the crossing chain is an attractive interaction between the deformed pancake stacks at large distances.[13] As a consequence, when the magnetic field is tilted from the layer direction, the density of the pancake stacks located on the Josephson vortices jumps from zero to a finite value. This means the existence of a maximum equilibrium separation a_m between pancake stacks, i.e., chains with $a > a_m$ are not realized in equilibrium. Note that the tilted vortices also attract each other within some range of angles and distances[7] meaning that tilted chains also have this property in some range of parameters.

A simple analytical formula for the attraction energy between the deformed pancake stacks can be derived for very anisotropic superconductors $\lambda_J \gg \lambda$ in the range $\lambda \ll R \ll \lambda_J$.[13] In this limit short-range pancake displacements u_n from the aligned positions in the two neighboring stacks produce a dipolelike contribution to the interaction energy per unit length between these stacks

$$\delta U_i(R) = -\frac{2\varepsilon_0}{NR^2}\sum_{n=1}^{N} u_n^2 = -\frac{2\varepsilon_0\langle u^2\rangle}{R^2}.$$

This term has to be combined with the usual repulsive interaction between straight stacks $U_{i0}(R) = 2\varepsilon_0 K_0(R/\lambda) \approx 2\varepsilon_0\sqrt{\pi\lambda/2R}\exp(-R/\lambda)$. Minimum of the total interaction energy, $U_{i0}(R) + \delta U_i(R)$, gives an estimate for the maximum equilibrium separation a_m,[13] $a_m = \lambda\ln(C\lambda^2/\langle u^2\rangle)$ and this result is valid until $a_m < \lambda_J$. Because in BSCCO λ_J is only 2–3 times larger than λ, this simple formula is not practical for this compound. We will see that a_m in BSCCO is usually larger than λ_J.

One can obtain a useful general recipe for determination of the maximum equilibrium separation between the pancake stacks directly from the chain energy per unit area E, without splitting it into the single-vortex and interaction parts. We consider situation when the in-plane component of the magnetic field is much larger than the lower critical field in this direction so that the in-plane magnetic induction practically coincides with the in-plane external magnetic field. The c component of the external field, H_z, determines the effective chemical potential μ for density of pancake stacks, $\mu = \Phi_0 H_z/(4\pi)$. With fixed chemical potential, the chain thermodynamic potential per unit area depends on pancake linear density n as

$$G(n) = E(n) - \mu n. \quad (35)$$

The equilibrium density n_μ is given by the minimum of this energy

$$\frac{dE(n)}{dn} = \mu.$$

Substituting this relation back to Eq. (35) we obtain

$$G(n_\mu) = E(n_\mu) - E'(n_\mu)n_\mu.$$

If we represent the energy as a function of the stack separation a rather than the density, the last result can be rewritten in a more compact way

$$G(a) = \frac{d}{da}[aE(a)].$$

The separation a in this formula corresponds an equilibrium separation only if $G(a)$ is smaller than the energy of the Josephson vortex lattice $G(\infty) \equiv E(\infty) = E_{JV}$. Therefore the maximum equilibrium separation a_m is given by the condition

$$\frac{dU(a)}{da} = 0, \tag{36}$$

where the quantity $U(a) = a[E(a) - E(\infty)]$ represents the pancake part of energy per one stack and the condition (36) implies that a_m is determined by the minimum of this energy. When the main contribution to the total interaction energy is coming from the nearest-neighbor interaction, a_m coincides with the position of the minimum in the pair interaction potential.

In principle, nonequilibrium structures with $a > a_m$ can be prepared by applying external stretching forces at the chain edges. However, the chain can be stretched only up to a certain critical value of separation. Above this value the system becomes unstable with respect to density fluctuations leading to formation of high-density chain clusters. The stability criterion of the chain is given by

$$\frac{d^2E(n)}{dn^2} > 0. \tag{37}$$

As

$$\frac{d^2E(n)}{dn^2} = a^3\frac{d^2}{da^2}\{a[E(a) - E(\infty)]\},$$

the stability criterion can also be written as

$$\frac{d^2U(a)}{da^2} > 0. \tag{38}$$

Therefore, in the dependence of the pancake part of energy per unit cell, U, on pancake separation a, the minimum gives the maximum equilibrium separation and the inflection point corresponds to the boundary of instability with respect to cluster formation.

As an example, we apply the obtained general formula (36) to the tilted chain at $\nu < \gamma$. Using Eqs. (30) and (17), we obtain from Eq. (36) a cubic equation for a_m

$$\frac{\tilde{a}_m^3}{N^2}(\ln N - 0.95) - \frac{\tilde{a}_m^2}{N}(\ln N - 0.41) + \tilde{a}_m - \pi\alpha = 0, \tag{39}$$

with $\tilde{a}_m \equiv a_m/\lambda_J$, which can be easily solved numerically in general case. At small α and large N an approximate solution of this equation gives

$$a_m \approx \pi\lambda\left[1 + \frac{\pi\alpha}{N}(\ln N - 0.41)\right],$$

i.e., at large N a_m approaches a remarkably simple universal value $\pi\lambda$.

VI. NUMERICAL EXPLORATION OF CHAIN STRUCTURES

A. Numerical implementation of the model

Our purpose is to calculate the equilibrium distribution of the regular phase $\phi_{r,n}(x,y)$ and pancake-row displacements on the basis of the energy (9). To facilitate numerical calculations, we introduce reduced variables

$$\tilde{y} = y/\lambda_J, \quad \tilde{x} = x/a, \; v_n = u_n/a$$

and represent the row interaction energy (10) in the reduced form

$$U_{Mr}(u,n) = \frac{\pi Ja}{\lambda^2}\tilde{\mathcal{V}}_{Mr}\left(\frac{u}{a}, n\right),$$

where $\tilde{\mathcal{V}}_{Mr}(v,n) = \mathcal{V}_{Mr}(v,n) - \mathcal{V}_{Mr}(0,n)$ and for $\mathcal{V}_{Mr}(v,n)$ we derive from Eq. (7)

$$\mathcal{V}_{Mr}(v,n) = \frac{s\lambda}{2a^2}\left[2\exp\left(-\frac{s|n|}{\lambda}\right)\ln[2\sin(\pi|v|)] + \sum_{m=-\infty}^{\infty} u\left(\frac{|v-m|}{\lambda/a}, \frac{s|n|}{\lambda}\right)\right]. \tag{40}$$

The reduced energy per unit area, $\tilde{E} = E\lambda_J/\varepsilon_0$, takes the form

$$\tilde{E} = \frac{1}{\pi N}\sum_{n=1}^{N}\int_0^{\tilde{a}}\frac{d\tilde{x}}{\tilde{a}}\int_{-\tilde{c}_y/2}^{\tilde{c}_y/2} d\tilde{y}\left\{\frac{1}{2}(\nabla\phi_{r,n})^2 + 1 - \cos[\nabla_n(\phi_{r,n} + \phi_{v,n}) - h\tilde{y}]\right\} + \frac{\tilde{a}}{2\alpha^2 N_{tot}}\sum_{n\neq m}\tilde{\mathcal{V}}_{Mr}(v_n - v_m, n-m) \tag{41}$$

with $h \equiv 2\pi B_x\gamma s^2/\Phi_0$ and $\tilde{a} = a/\lambda_J$. The reduced local energy is defined as

$$\tilde{E}_{loc} = \tilde{E} - \frac{\pi\tilde{c}_y}{6N^2}. \tag{42}$$

In particular, from Eqs. (21) and (31) we obtain the following results for the reduced local energies of two limiting configurations in the limit $\tilde{a}/N = \nu/\gamma \ll 1$

$$\tilde{E}_{loc} \approx \begin{cases} \dfrac{\ln N + C_{JV}}{N} - \dfrac{8\alpha^2}{N\tilde{a}\ln(3.5/\alpha)}, & \text{for crossing chain} \\ \dfrac{1}{\tilde{a}}U\left(\dfrac{\tilde{a}}{2\pi\alpha}\right) + \dfrac{\tilde{a}}{2N^2}(\ln N - 0.95), & \text{for tilted chain.} \end{cases} \tag{43}$$

We will also use the excess pancake part of energy defined as

$$\delta E \equiv E - E_{JV} \tag{44}$$

$$= (\lambda_J/\varepsilon_0)(E - E^s_{PS} - E_{JV}) \tag{45}$$

with E_{JV} being the JV lattice energy per unit area and the excess pancake energy per stack (in units of ε_0), $\tilde{U} \equiv \tilde{a}\delta\tilde{E}$.

The phase distribution $\phi_{r,n}$ and pancake displacements v_n minimizing the energy functional (41) obey the following equations:

$$\Delta\phi_{r,n} + \sin[\nabla_n(\phi_{r,n} + \phi_{v,n}) - h\tilde{y}] - \sin[\nabla_n(\phi_{r,n-1} + \phi_{v,n-1}) - h\tilde{y}] = 0, \tag{46a}$$

$$\nabla_y\phi_{rn}(v_n\tilde{a},0) + \frac{\tilde{a}}{2\alpha^2}\sum_{m=-\infty}^{\infty}\mathcal{F}_{Mr}(v_n - v_m, n-m) = 0, \tag{46b}$$

where $\mathcal{F}_{Mr}(v,n) \equiv -\nabla_v\mathcal{V}_{Mr}(v,n)$ is the magnetic interaction force between the vortex rows

$$\mathcal{F}_{Mr}(v,n) = -\frac{\pi s\lambda}{a^2}\exp\left(-\frac{s|n|}{\lambda}\right)\cot\pi v + \frac{s\lambda}{a^2}\sum_{m=-\infty}^{\infty}\frac{1}{v-m}\exp\left[-\frac{\sqrt{(v-m)^2 + s^2n^2}}{\lambda/a}\right]. \tag{47}$$

Note that both $\mathcal{V}_{Mr}(v,n)$ and $\mathcal{F}_{Mr}(v,n)$ are regular at $v \to 0$, because divergency in the first term is compensated by the $m=0$ term in the sum.

In numerical calculations we assume for simplicity periodic boundary condition in y direction with period c_y. Physically, this corresponds to rectangular arrangement of both Josephson vortices and pancake stacks. Even though such arrangement does not give the true ground state, it does not influence much the structure of an individual chain, that is the focus of this paper. Due to symmetry properties, it is sufficient to find the phase distribution $\phi_n(x,y)$ within domain $0<x<a$, $0<y<c_y/2$, $1\leqslant n\leqslant N_l = N/2$ with the following boundary conditions for the total phase:

$$\phi_n(a+0,y) = \phi_n(+0,y), \quad \phi_n(x,-0) = \pi - \phi_n(x,+0),$$

$$\phi_n\left(x,\frac{c_y}{2}+0\right) = -\phi_n\left(x,\frac{c_y}{2}-0\right) + \frac{2\pi(n-1/2)}{N},$$

$$\phi_0(x,y) = -\phi_1(-x,y), \quad \phi_{N_l+1}(x,y) = \pi - \phi_{N_l}(x,y).$$

Pancake displacements v_n have symmetry properties $v_{n+N} = v_n$ and $v_{1-n} = -v_n$. This allows us to reduce infinite m summation in Eq. (46b) to summation over half of the unit cell $1\leqslant m\leqslant N_l$

$$\sum_{m=-\infty}^{\infty}\mathcal{F}_{Mr}(v_n - v_m, n-m) = \sum_{m=1}^{N_l}\sum_{l=-\infty}^{\infty}[\mathcal{F}_{Mr}(v_n - v_m, n-m+lN) + \mathcal{F}_{Mr}(v_n + v_m, n+m-1+lN)].$$

Similar decomposition was made for the magnetic interaction energy in Eq. (41).

We explored chain phase structures by numerically solving Eqs. (46) with respect to the pancake-row displacement v_n and regular phase distribution $\phi_{r,n}$ for different values of the parameters a, $N=2N_l$, and α. Numerical computations were performed on two Linux workstations with 2 GHz AMD Athlon processors and on the nodes of the Argonne computing cluster "Jazz" (350 nodes, each with 2.4 GHz Pentium Xeon processor). In the following sections we review the results of these calculations.

B. Stability of crossing configuration

The fundamental property of the crossing-chain state is the structure of the crossing configuration of Josephson vortex and pancake stack. In-plane currents of the Josephson vortex displace the pancakes in the opposite directions above and below central layers. Equilibrium displacements are the result of a balance between the pulling forces of the Josephson vortex, which try to tear the pancake stack apart, and magnetic coupling, which tries to keep the stack aligned. The structure of the crossing configuration can be calculated analytically in the regime of high anisotropy $\lambda \ll \lambda_J$[8,19] leading to the result (18) for the crossing energy and to the maximum displacement $u_1 \approx 2.2\lambda^2/[\lambda_J \ln(2\lambda_J/\lambda)]$. This calculation is based on (i) quadratic approximation for the magnetic tilt energy and (ii) assumption that the JV in-plane currents are not influenced much by pancake displacements. The first assumption breaks down when u_1 approaches λ and the second one breaks down when u_1 become comparable with λ_J. This means that the both approximations break down as λ approaches λ_J.

The stability of the crossing configuration has been addressed recently by Dodgson[21] using the full magnetic coupling energy but without taking into account modification of the Josephson vortex by pancake displacements. The latter can not be easily computed analytically. This calculation suggested that the crossing configuration becomes unstable at $\alpha \equiv \lambda/\lambda_J \approx 1/2.86 \approx 0.35$. This estimate seems to be in contradiction with the recent decoration experiments[22] where the isolated pancake stacks sitting on the Josephson vortices have been observed in the strongly overdoped BSCCO with the ratio α significantly larger than this value.

To resolve this contradiction and find an accurate stability criterion we studied numerically evolution of the isolated crossing configuration with increasing ratio α. For this purpose we used the code, which calculates the chain structure in Fig. 1, for large values of the periods a and $N=2N_l$. Figure 2(a) shows the dependence of the maximum pancake displacement on the ratio α for $N=20$ and different values of a. One can see that the crossing configuration becomes unstable near $\alpha \approx 0.69$, which significantly exceeds a simple estimate in Ref. 21. The main reason for the extended stability range

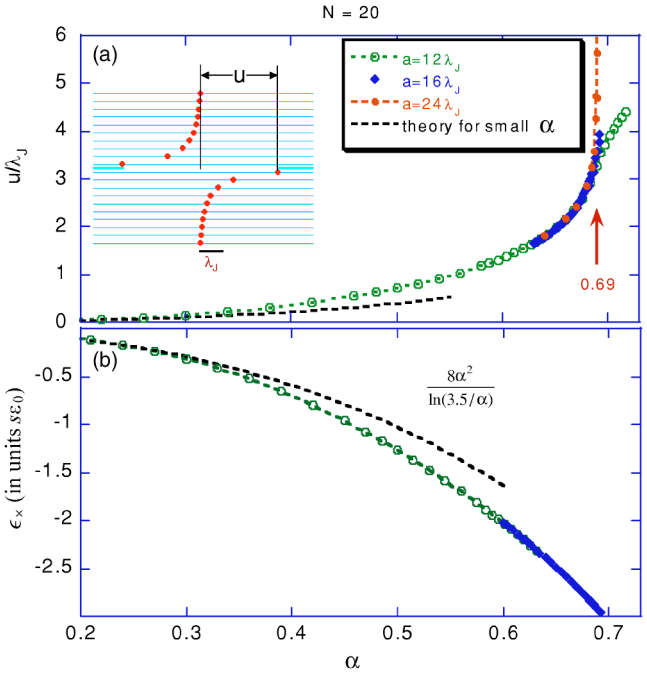

FIG. 2. (Color online) (a) The dependence of the maximum pancake displacement in the crossing (defined in the inset) on the ratio $\alpha=\lambda/\lambda_J$ for different periods a in x direction. The plot shows that crossing becomes unstable near $\alpha=0.69$. The inset shows crossing configuration near instability point. (b) The dependence of crossing energy on the ratio α. For comparison, small-α calculation is shown in both plots.

is that the pancake displacements significantly modify the structure of the Josephson vortex. This reduces forces which pull the pancake stacks away and compensates for reduced magnetic coupling restoring forces at large u. Finite-size effect is only noticeable in vicinity of the instability. The small-α calculation correctly predicts the maximum displacement up to $\alpha\approx 0.35$ and underestimates it at larger α. Figure 2(b) shows the α dependence of crossing energy $\epsilon_\times$. It demonstrates a rather regular behavior almost up to the instability point. Similar to the maximum displacement, the small-α calculation gives an accurate estimate for $\epsilon_\times$ up to $\alpha\approx 0.35$. For higher α an absolute value of $\epsilon_\times$ exceeds the analytical estimate.

C. Typical phase diagram within the range $0.4\lesssim\alpha\lesssim 0.5$: Phase transition from crossing to tilted chains with decreasing pancake separation

At the first stage we studied the evolution of chain structures with increasing $\alpha\equiv\lambda/\lambda_J$ for fixed periods a and N. As λ increases with the temperature and λ_J is approximately temperature independent, increase of α corresponds to increase of the temperature in real systems except that our calculations do not take into account thermal fluctuations. For small values of a and N we found that the chain structure evolves smoothly. An example of such evolution is presented in Fig. 3 for $N=14$ and $a=1.52\lambda_J$. The main plot shows the dependence of the maximum pancake displacement from the straight-stack position u_{max}/a (defined in the inset) on the parameter α. We will use this ratio to characterize the chain structure throughout the paper. It changes from zero for straight stacks to $(1-1/N)/2$ for tilted chains. At small α a

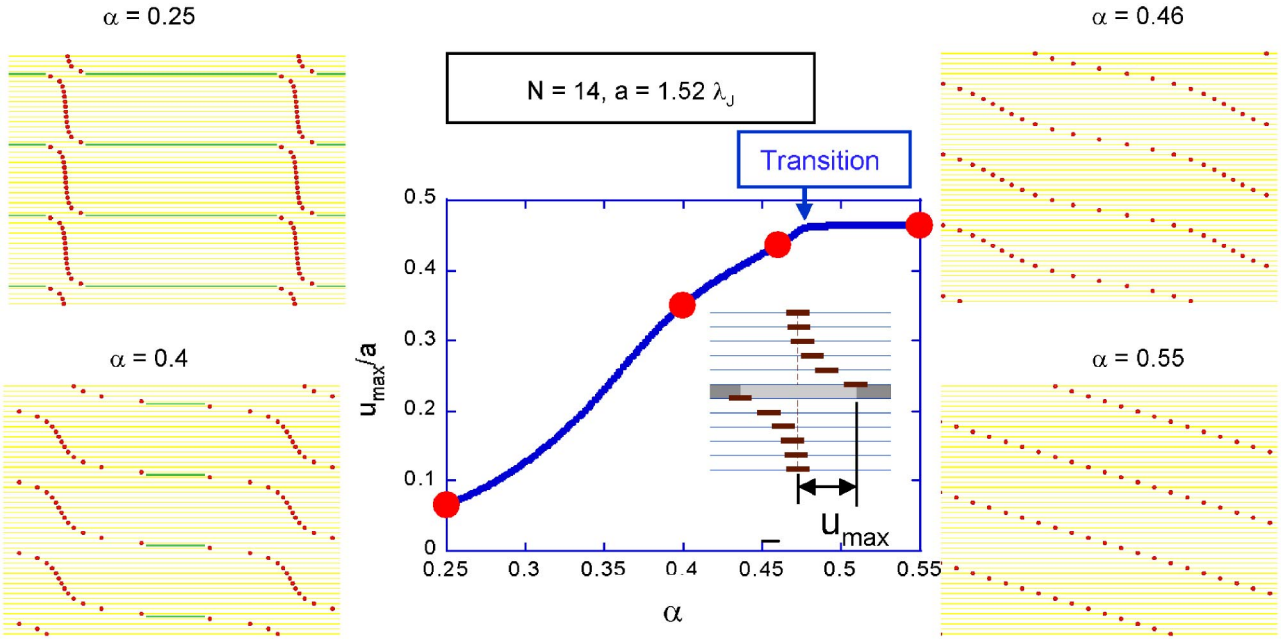

FIG. 3. (Color online) *Main plot* shows the dependence of the maximum displacement(defined in the inset) divided by pancake separation on the parameters α for $N=14$ and $a=1.52\lambda_J$. The chain structures are illustrated at marked points. In the configuration pictures circles show positions of the pancake vortices and horizontal lines mark locations of the Josephson vortices. One can see that the system evolves from weakly deformed chain ($\alpha=0.25$) via strongly deformed chain ($\alpha=0.4$) to modulated tilted chain ($\alpha=0.46$). The last structure transforms via a second-order phase transition at $\alpha=0.48$ into tilted straight vortices.

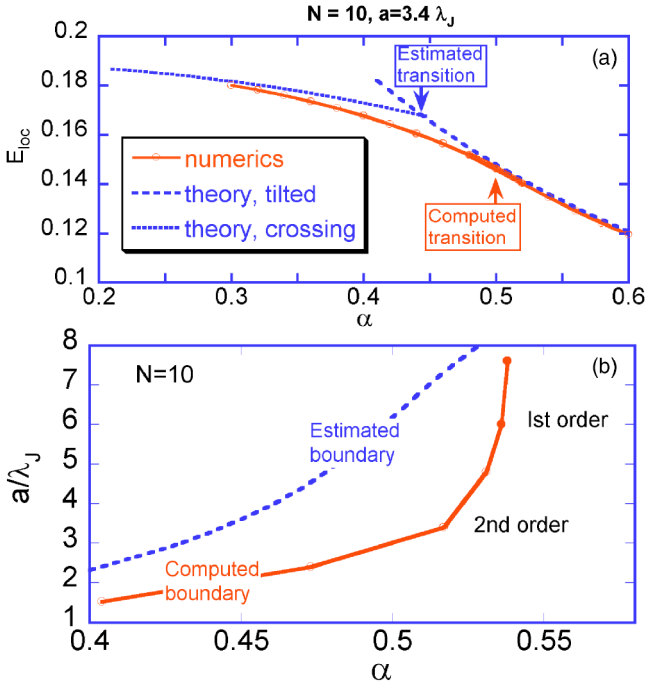

FIG. 4. (Color online) (a) The dependence of the local part of energy of the chain configuration on the ratio α for $N=10$ and $a=3.4\lambda_J$. For comparison, we also show analytical estimates for the crossing and tilted chain configuration. (b) Phase diagram in the plane (pancake separation a)-(ratio α) for the fixed separation between JVs, $N=10$. The solid line shows computed transition into the tilted chain state. The dashed line shows location of the transitional region where the energy of the crossing configuration is equal to the energy of the tilted configuration.

weakly deformed crossing configuration is always realized (see the structure at $\alpha=0.25$). The pancake displacements grow with increasing α and the chain evolves into strongly corrugated configurations such as configuration for $\alpha=0.4$ in Fig. 3. With further increase of α, this structure smoothly transforms into modulated tilted lines (see the structure for $\alpha=0.46$). Finally, the last structure transforms via a second-order phase transition into the straight tilted lines. For parameters used in Fig. 3 this occurs at $\alpha=0.48$. The plateau in the dependence $u_{max}(\alpha)$ above this value of α corresponds to the maximum displacement $(1-1/N)/2$ in the tilted chain.

To compare numerical and analytical calculations we plot in Fig. 4(a) the numerically computed α-dependence of the local energy (42) together with analytical estimates (43) for $N=10$ and $a=3.4\lambda_J$. One can see that the analytical estimates accurately reproduce numerical results for the weakly deformed crossing chain at $\alpha<0.35$ and for the tilted chain at $\alpha>0.5$. However, in between the numerical study predicts intermediate configurations with energies smaller than the energies of the both limiting configurations. As a result, a naively expected first-order phase transition is replaced by a continuous transition occurring at significantly larger α. This behavior is quite general. We observed it within the broad range of the periods, $6\lesssim N\lesssim 20$, $2\lesssim a/\lambda_J\lesssim 5$ and the ratios $0.4\lesssim\alpha\lesssim 0.6$. In Fig. 4(b) we compare location of the phase transition into the tilted-chain state in the a-α plane for $N=10$ with location of the transitional region defined by Eq.

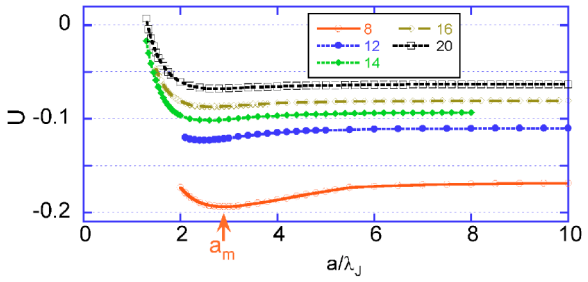

FIG. 5. (Color online) The dependence of the excess pancake energy per stack in units of ε_0, U, on the separation between pancakes a for $\alpha=0.5$ and different N. The position of minimum of this energy corresponds to the maximum equilibrium separation a_m (marked for $N=8$ plot).

(33). The computed transition line is always displaced from the estimated boundary in the direction of larger α. The transitional region just marks the location of the intermediate strongly deformed chain configurations. The observed continuous phase transition indicates that tilted lines become unstable with decrease of α. It is known that an isolated vortex line in anisotropic superconductors is unstable within some range of tilt angles.[24,25] We have to note that the stability criterion of a chain is not identical to the stability criterion of an isolated vortex line and requires separate study. At large values of a a continuous transition is replaced by a first-order phase transition. However, as it was discussed in Sec. V, due to the attractive interaction between the pancake stacks, large separations may not realize in equilibrium because a is expected to jump from infinity to the maximum equilibrium separation a_m.

To find location of a_m in the phase space, we calculated the evolution of chain structures with changing a for fixed α and N. These calculations, of course, reproduce the chain structures and location of the transition line of the previous calculation. Following the recipe of Sec. V, we calculated the a dependence of the excess pancake energy per unit stack, $U(\tilde{a})\equiv\tilde{a}(E-E_{JV})$, and find a_m from the minimum location of this energy. Figure 5 shows an example of these dependencies for $\alpha=0.5$ and different N. Increasing $U(a)$ at $a>a_m$ implies attractive interaction between stacks at large separations. We can see that for $\alpha=0.5$ the separation a_m weakly depends on N and lies in between $2\lambda_J$ and $3\lambda_J$. Note that the N dependence of the limiting value of $U(a)$ at $a\to\infty$ reflects contribution from the crossing energy of an isolated pancake stack with the JV array.

In Fig. 6 we present the chain phase diagrams in the a-N plane for two values of α, 0.4 and 0.5. Solid lines show the phase transition into the tilted-chain state [the dependence $a_t(N)$]. One can see that at larger N the transition takes place at smaller a. With increasing α this line moves higher meaning that the tilted-chain state occupies larger area in the phase space. At large a weakly deformed chain configurations are realized, similar to ones shown in Fig. 3 for $\alpha=0.25$. With decreasing a the chain configuration crosses over into a strongly corrugated state. To mark location of this crossover we show in the phase diagrams by dashed lines the pancake separation at which the maximum pancake displacement u_{max} reaches $a/4$ [plot $a_r(N)$]. This crossover can be

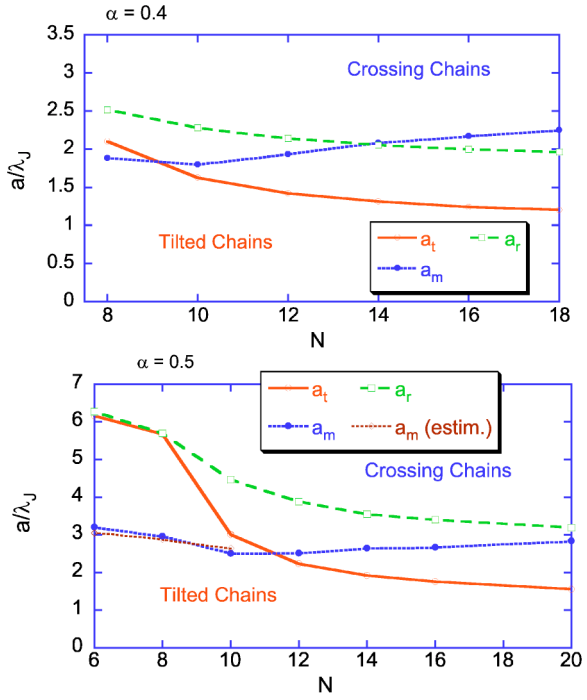

FIG. 6. (Color online) Chain phase diagrams in the plane $a/\lambda_J - N$ for two values of the ratio α, 0.4 and 0.5. The solid line indicate phase transition into the tilted-chain phase. The dotted line shows the maximum equilibrium separation a_m. The dashed line shows crossover "reconnection" line at which the maximum displacement exceeds $a/4$ and weakly deformed crossing configuration crosses over into the strongly corrugated configuration. For $\alpha = 0.5$ we also show a_m for the tilted-chain phase analytically calculated from Eq. (39).

viewed as "reconnection" of pancake-stack segments. Dotted lines show locations of a_m. We see that $a_m(N)$ line crosses the transition line meaning that at small N a_m falls into the tilted-chain region and at large N it falls into the crossing-chains region. For $\alpha = 0.5$ we also show the analytical estimate for a_m for the tilted chain calculated from Eq. (39). One can see that it agrees very well with numerical calculations. For $\alpha = 0.5$ and $N \leqslant 8$ the transition is of the first order. However, the pancake separation at the transition lies above a_m meaning that it does not correspond to the ground state.

The obtained phase diagrams imply that at small tilting angle of the field with respect to the c axis (corresponding to small a) the tilted chains have lower energy than the crossing chains. This is similar to the situation at higher fields, in the dense lattice, where the crossing-lattices state also is expected to transform into the simple tilted lattice at small tilting angle of the field.[8]

D. Typical phase diagram in the range $0.5 \lesssim \alpha \lesssim 0.65$: Reentrant transition to kinked/tilted lines at small concentration of pancake vortices

At higher values of the ratio α an additional qualitative feature emerges in the phase diagram. When α exceeds the characteristic value, a small c-axis field penetrates superconductor in the form of kinks forming kinked vortex lines (lock-in transition, see, e.g., Refs. 3–5). The critical value of α is determined by combination of numerical constants in the pancake-stack and kink energies and it is given by $\alpha_c = \exp C_{kv}$, where the constant C_{kv} is defined after Eq. (26). To find the value of α_c, we calculated in Appendix A the energy of tilted chains at very large pancake separations a, which allowed us to extract the energy of an isolated kink. This calculation gives $C_{kv} \approx -0.81$ corresponding to $\alpha_c \approx 0.44$. It is important to note that the critical value of α increases with decrease of N, due to the increasing contribution of the crossing energies to the total energy of crossing chain. Very interesting behavior is expected when α is only slightly larger than α_c. The competing chain states have very different interactions: deformed stacks attract and kinks repel each other. Moreover, at the same value of the c-axis magnetic induction, B_z, the kink separation is much smaller than the stack separation and the absolute value of the kink interaction energy is much larger than the interaction energy between deformed stacks. As a consequence, with increasing B_z the total energy of the kinked lines rapidly exceeds the total energy of the crossing chain and the system experiences a first-order phase transition into the crossing-chain state. Due to the attractive interaction between the pancake stacks, the pancake/kink separation at which the energy curves cross does not give the equilibrium separation for the crossing chain and the stack separation jumps at the transition to a value slightly smaller than the maximum equilibrium separation a_m. This means that the phase transition is accompanied by jump of pancake density and magnetic induction, B_z.

This behavior was confirmed by numerical calculations. Figure 7 shows a plot of the dependence of the pancake energy U on the pancake separation for $N=16$ and $\alpha=0.6$. This dependence has two branches, corresponding to the two different starting states at large a, crossing chain and kinked lines. This branches cross at $a=14.8\lambda_J$ and the the kinked vortex lines have smaller energy at larger a. The variations of U at large a occur due to the interaction energy and one can see that the kink interaction energy is much larger than the interaction energy of the deformed stack in the crossing chain. With further decrease of a, the crossing chain smoothly transforms into the tilted chain, as it was described in the previous section. The second-order phase transition for these parameters takes place at $a \approx 2.5\lambda_J$ somewhat smaller than the maximum equilibrium separation $a_m \approx 3.44\lambda_J$.

The pancake separation (or pancake density) in the chain cannot be directly fixed in experiment. Instead, the magnetic field strength, H_z, fixes the chemical potential μ_H, $\mu_H = \Phi_0 H_z/(4\pi)$, and the equilibrium density is determined by the global minimum of the thermodynamic potential $G(n) = E(n) - \mu_H n$. To find evolution of density with increasing chemical potential, we plot in Fig. 8 the density dependencies of the reduced thermodynamic potential, $\delta E - \mu n$ for different μ and representative parameters $N=14$ and $\alpha=0.6$. As the energy of isolated stacks is subtracted in δE, the dimensionless chemical potential is shifted with respect to its bare value and it is related to the magnetic field strength as

$$\mu = \frac{\Phi_0 (H_z - H_{c1})}{4\pi\epsilon_0},$$

where H_{c1} is the lower critical field for $\mathbf{H} \| c$. We find that for selected parameters the transition takes place at

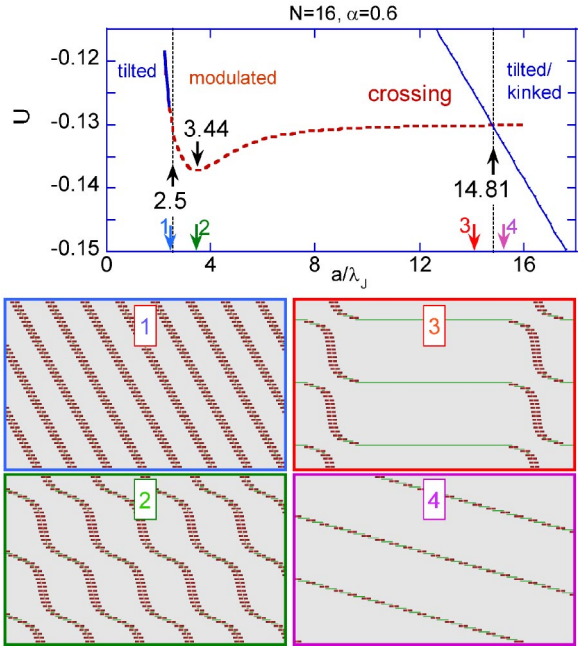

FIG. 7. (Color online) The dependence of the excess pancake energy per stack on pancake separation a for $N=16$ and $\alpha=0.6$. The two branches correspond to the two different starting states at large a, crossing chain and kinked lines. One can see that the kinked lines have lower energy at very large a, $a>14.81$. Crossing chain smoothly transforms back into tilted chain with decrease of a. The transformation is completed at a second-order phase transition point at $a_t=2.5\lambda_J$. Chain configurations at four points marked by arrows are shown below. The evolution of chain configuration along this energy curve is also illustrated by an animation (See Ref. 26).

$\mu=\mu_t=-0.152$. At $\mu<\mu_t$ the global minimum falls into the region of kinked lines and at $\mu>\mu_t$ it jumps into the region of crossing chain. Note that the density value, at which the energy curves cross (kinks in the lines near $n=0.1$ in Fig. 8), is always larger than the lower density from which the jump to the high-density state takes place. At the transition, the density jumps almost ten times, from $0.037/\lambda_J$ to $0.315/\lambda_J$.

The numerically obtained phase diagram in the N-a plane for $\alpha=0.6$ is shown in the upper panel of Fig. 9. The plots in the lower left panel, the thermodynamic potential at the transition point and the maximum displacement versus a/λ_J, illustrate definitions of different lines in the phase diagram. The lines 1 and 1′ show the limiting pancake separations at the first-order transition between which the jump takes place. When the chemical potential is fixed by external conditions, the area between these lines is bypassed in equilibrium. At large N the jump takes place from the kinked-lines state into the strongly corrugated configuration. This configuration transforms into the tilted chain with further decrease of a via continuous transition shown by the line 2′. Below $N=14$ only tilted chains realize, but the density jump still exists. The upper separation grows approximately proportional to N while the lower separation slowly decreases with N and lies slightly below the maximum equilibrium separation a_m shown by dotted line. This means that the relative density jump increases with N. The line 2 shows the position of the crossing of the energy curves for the two states.

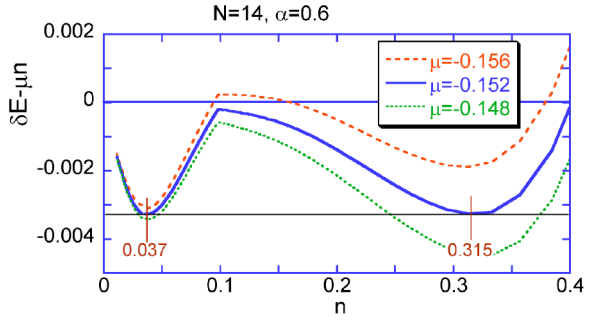

FIG. 8. (Color online) The density dependence of the pancake part of the thermodynamic potential per unit area, $\delta E-\mu n$ (in units of ϵ_0/λ_J) at different chemical potentials μ corresponding to different values of the magnetic field strength for $N=14$ and $\alpha=0.6$. Kinks in the curves separate regions of tilted/kinked lines (low n) and crossing chains (high n). The equilibrium density in units of $1/\lambda_J$ is given by the global minimum of this energy. One can see that at $\mu\approx-0.152$ the system experiences a first-order phase transition with very large density jump.

It is also instructive to examine the phase diagram for fixed c-axis period N, in the a-α plane. As α increases with temperature, this diagram to some extent describes the temperature evolution of the chain structure. Figure 10 shows

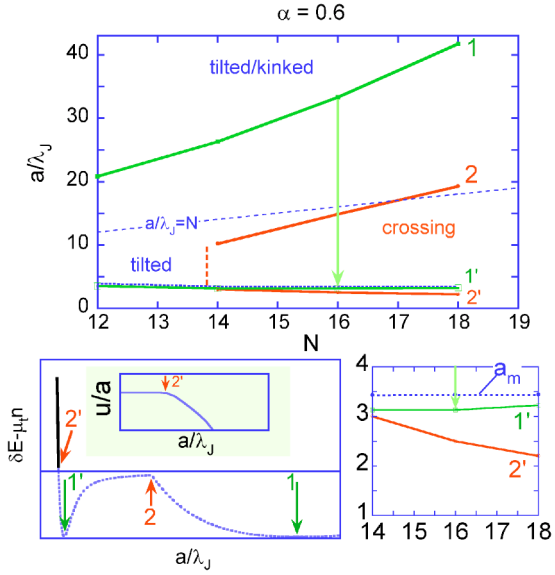

FIG. 9. (Color online) *The upper plot* shows the phase diagram in the N-a plane for $\alpha=0.6$. The left plot in the lower plat illustrates meanings of the phase lines using the plot of the thermodynamic potential $\delta E-\mu n$ vs a/λ_J at the transition point (main plot) and the maximum displacement u divided by lattice spacing a vs a/λ_J (inset). The lines 1 and 1′ correspond to the two limiting pancake separations at the transition point between which the jump occurs. The line 2 indicates crossing of the energy curves for the kinked and crossing chain. The line 2′ shows the position of a continuous transition into the tilted chain (illustrated by the inset in the lower panel). Dotted line slightly above 1′ line shows the position of the maximum equilibrium separation a_m. We also show the crossover line $a/\lambda_J=N$ above which well-defined kinks appear. The right plot in the lower part shows blowup of the phase diagram above the 2′ line.

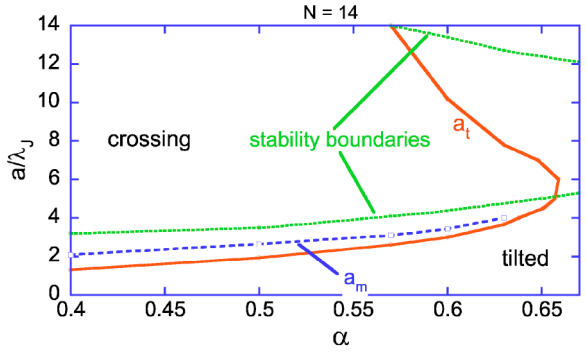

FIG. 10. (Color online) Phase diagram in a-α plane for $N=14$. Solid nose-shaped line shows the phase transition into the tilted-chain state. Dashed line shows location of the maximum equilibrium separation, which terminates at some point. We also show by dotted line location of the stability boundaries obtained from inflection points of the dependencies $U(a)$ [see criterion (38)].

such diagram for $N=14$. One can see that the phase transition line is reentrant, within some range of α the tilted chains are realized both for small and large a. Above some critical value of α (0.66 for $N=14$) only straight tilted lines exist in whole range of a. This maximum value increases with N. For somewhat smaller values of α, there is narrow range of a where the chains become slightly modulated. This is illustrated in the plot of the maximum displacement u for $\alpha=0.63$ in the right panel of Fig. 11. The maximum equilibrium separation line $a_m(\alpha)$ terminates at certain value of α, above which the dependence $U(a)$ becomes monotonic. We also show in this diagram the stability boundaries extracted from the inflection points in the $U(a)$ dependencies [see criterion (38) and related discussion]. Origin of such phase diagram can be better understood by studying the dependencies $U(a)$ at different α shown in the left panel of Fig. 11. One can see that the first-order transition vanishes above certain value of α and the dependence $U(a)$ becomes monotonic

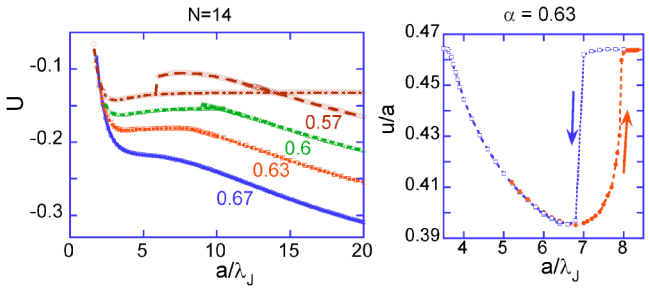

FIG. 11. (Color online) *Left panel*: The dependencies of the excess pancake energy per stack U on separation a for $N=14$ and different values of α. With increasing α the first-order transition from tilted to crossing chain vanishes and the crossing chain do not realize at all. Also the dependence $U(a)$ becomes monotonic which corresponds to termination of $a_m(\alpha)$ line in Fig. 10. *Right panel*: The dependence of the relative maximum displacement u on separation a for $N=14$ and $\alpha=0.63$. The maximum value of u, corresponding to tilted chains, is given by $(1-1/14)/2\approx 0.464$. One can see that there is a range of a where the chains become only slightly modulated.

close to this value of α. On the other hand, even after becoming monotonic, this dependence still has two inflection points bounding unstable region in some range of a. Existence of such unstable region means that the pancake-density jump with increasing the c-axis external field persists in the region where only tilted chains exist. This jump is closely related (but not identical) with the jump of the tilt angle of the vortex line at the lower critical field with increasing tilt angle of the external field.[27,28]

The vortex chains in BSCCO at small concentrations of pancakes have been studied by the scanning Hall probe microscopy in Ref. 14. It was found that at very small concentration of pancakes the chains are magnetically homogeneous and separate pancake stacks are not resolved. When the external field exceeds certain critical value, crystallites of the pancake stacks are suddenly formed along the chains and the flux density in crystallites approximately ten times higher then the flux density in homogeneous chains. The (kinked lines)-(crossing chains) first-order phase transition provides a very natural explanation for this observations.

VII. CONCLUSIONS

In conclusion, we investigated numerically and analytically the phase diagram of an isolated vortex chain in layered superconductors. In the region where Josephson and magnetic coupling are approximately equal, we found a very rich behavior. The crossing chains typically transform into tilted chains with decreasing pancake separation via formation of intermediate strongly deformed configurations and a continuous phase transition. When the relative strength of the Josephson coupling exceeds some typical value, the phase diagram becomes reentrant. At a very small c-axis field, tilted chains are realized in which the vortex lines have the kinked structure. With increasing c-axis field these low-density tilted chains transform via a first-order phase transition into strongly deformed crossing chains. This transition is accompanied by a large jump of the pancake-vortex density. With further increase of the field these crossing chains transforms back into the tilted chains via a second-order transition.

An important feature of real BSCCO which is not taken into account in this paper is the thermal vortex fluctuations. We expect that fluctuations will not change qualitatively the described behavior, especially the strong first-order phase transition, but may significantly change locations of the phase transitions in the phase space.

Finally, we briefly overview the relevant field scales. In the range of studied JV separations, N, from 10 to 20, and for $\gamma=500$, the in-plane field, $B_x=2\Phi_0/(\sqrt{3}\gamma s^2N^2)$, varies in the range from 200 to 50 G and the in-plane separation between Josephson vortices, $c_y=(\sqrt{3}/2)\gamma sN$, varies from 6.75 to 13.5 μm. The typical density jump for $N=16$ and $\alpha=6$ in Fig. 9 corresponds to jump of the average c-axis induction, $B_z=\Phi_0/ac_y$, from 0.12 to 1.2 G. Such jump is usually difficult to notice in the global magnetization measurements. Therefore, a rich spectrum of transformations discussed in this paper takes place in the range of very small c-axis magnetic induction, not exceeding few gauss. Taking a typical value λ for BSCCO at 80 K, as 0.4 μm, we

estimate for the same parameters that the maximum *c*-axis field in the chain center, $B_{z0}=\Phi_0/a\lambda$, jumps from 3.3 to 33 G.

ACKNOWLEDGEMENTS

I would like to thank M. Dodgson, A. Grigorenko, S. Bending, and V. Vlasko-Vlasov for useful discussions. I also gratefully acknowledge use of Jazz, a 350-node computing cluster operated by the Mathematics and Computer Science Division at Argonne National Laboratory as part of its Laboratory Computing Resource Center. This work was supported by the U. S. DOE, Office of Science, under Contract No. W-31-109-ENG-38.

APPENDIX A: KINK INTERACTION ENERGY OF A SINGLE LINE

We compute the kink interaction energy within London approximation. As the main contribution to this energy comes from the regions away from the JV and kink cores, one can expect that the London approach gives a very good approximation of the interaction energy. Shape of the kinked line is given by

$$\mathbf{R}(X)=[X,0,u(X)],$$

$$u(X)=ns, \quad (n-1/2)L<X<(n+1/2)L.$$

From the general formula (8) we obtain the total energy of the kinked line in London approximation

$$\varepsilon_{\rm kl}=\frac{\Phi_0^2}{8\pi L_x}\int\frac{d^3\mathbf{k}}{(2\pi)^3}\int dX\int dX' \times\frac{(1+\lambda^2k^2)+(1+\lambda_c^2k^2)\frac{du}{dX}\frac{du}{dX'}}{(1+\lambda^2k^2)(1+\lambda^2k_z^2+\lambda_c^2k_\parallel^2)} \times\exp[ik_x(X-X')+ik_z(u-u')]. \tag{A1}$$

To separate the kink interaction energy one has subtract from this expression the energies of Josephson vortices, ε_{JV}^L, and kinks, $\varepsilon_{\rm kink}^L$, in London approximation. Integration over X, X', and k_x leads to the following expression for the total kink contribution to energy, $\varepsilon_k=\varepsilon_{\rm kl}-\varepsilon_{JV}^L$:

$$\varepsilon_k=\frac{\Phi_0^2}{8\pi}\int\frac{dk_ydk_z}{(2\pi)^2}\left[\left(\frac{1}{1+\lambda^2k_z^2}-\frac{1}{1+\lambda^2k_z^2+\lambda_c^2k_y^2}\right)\times\frac{\sinh g}{g}\frac{1-\cos(k_zs)}{\cosh g-\cos(k_zs)}+\frac{s^2/\lambda^2}{2(1+\lambda^2k_z^2)}\frac{\sinh g_1/g_1}{\cosh g_1-\cos k_zs}\right]$$

with

$$g=L\sqrt{\lambda_c^{-2}+\gamma^{-2}k_z^2+k_y^2},$$

$$g_1=L\sqrt{\lambda^{-2}+k_y^2+k_z^2}.$$

To separate kink interaction we have to subtract the contribution coming from isolated kinks, i.e., the term which behaves as $1/L$ at $L\to\infty$

$$\varepsilon_{\rm kink}^L=\frac{\Phi_0^2}{8\pi}\int\frac{dk_ydk_z}{(2\pi)^2}\left[-\frac{1-\cos(k_zs)}{g(1+\lambda^2k_z^2+\lambda_c^2k_y^2)}+\frac{s^2}{2\lambda^2(1+\lambda^2k_z^2)}\left(\frac{1}{g_1}+\frac{\lambda^2k_z^2}{g}\right)\right].$$

This gives the following result for the kink interaction energy:

$$\varepsilon_{\rm ki}=\frac{\Phi_0^2}{8\pi}\int\frac{dk_ydk_z}{(2\pi)^2}\left[\left(\frac{1}{1+\lambda^2k_z^2}-\frac{1}{1+\lambda^2k_z^2+\lambda_c^2k_y^2}\right)\times\frac{1-\cos(k_zs)}{g}\frac{\cos k_zs-\exp(-g)}{\cosh g-\cos k_zs}+\frac{s^2/\lambda^2}{2(1+\lambda^2k_z^2)}\frac{1}{g_1}\frac{\cos(k_zs)-\exp(-g_1)}{\cosh g_1-\cos(k_zs)}\right], \tag{A2}$$

which has to be evaluated in the limit $L>\gamma s$. The main contribution is coming from the first term in square brackets. If we keep only this term, than the kink interaction energy can be reduced to the following form:

$$\varepsilon_{\rm ki}\approx\frac{\gamma\Phi_0^2s^2}{8\pi\lambda^2L^2}J(L/\lambda_c)$$

with

$$J(r)=\int\frac{dp_ydp_z}{(2\pi)^2}\left(\frac{1}{1+p_z^2}-\frac{1}{1+p^2}\right)\times\frac{p_z^2}{\sqrt{1+p^2}}\frac{r}{\exp(r\sqrt{1+p^2})-1},$$

$$p^2\equiv p_y^2+p_z^2.$$

In the practically interesting case $r=L/\lambda_c\ll1$ the integral $J(r)$ can be evaluated as

$$J\approx\frac{1}{4\pi}\left[\ln\left(\frac{1}{r}\right)-\frac{3}{2}\right],$$

giving the main result for the kink interaction energy (25).

The second term in square brackets of Eq. (A2) represents magnetic coupling contribution to the kink interactions. We calculated this contribution in the two limiting cases

$$\varepsilon_{\rm ki}^{(2)}\approx\begin{cases}\dfrac{s^2\varepsilon_0}{L^2}, & \text{for } L\ll\lambda\\[2ex] \dfrac{s^2\varepsilon_0}{\lambda L}\exp(-L/\lambda), & \text{for } L\ll\lambda\end{cases}.$$

As we can see, it does give a very small contribution to the total kink interaction energy.

APPENDIX B: DERIVATION OF THE INTERACTION ENERGY OF TILTED VORTICES

The interaction potential between two straight tilted vortices per unit length along c-axis separated by distance R in the tilt direction (x axis) is given by

$$U_i(R) = \frac{\Phi_0^2}{4\pi}\int \frac{dk_x dk_y}{(2\pi)^2} \times \frac{\nu^2 + [1+\lambda_c^2(k_\perp^2+\nu^2k_x^2)]/[1+\lambda^2(k_\perp^2+\nu^2k_x^2)]}{1+\lambda^2\nu^2k_x+\lambda_c^2k_\perp^2} \times \exp(ik_xR)$$

This formula works also in the regime of kinked vortex lines $\nu > \gamma$. The kink structure of the lines starts to influence interaction between them when kink separation L exceeds $c_z\gamma/2\pi$ corresponding to the condition $\nu > N\gamma/2\pi$. Integrating over k_y we obtain $U_i(R) = \int (dk/2\pi)\cos(kR)U_i(k)$ with

$$U_i(k) = 2\pi\varepsilon_0\lambda\sum_{j=1}^{3} g_j(k) \tag{B1}$$

with

$$g_1(k) = \frac{\nu^2\lambda^2+\lambda_c^2}{\lambda_c[1+(\nu^2\lambda^2+\lambda_c^2)k^2]^{1/2}},$$

$$g_2(k) = -\frac{\lambda_c}{[1+(\nu^2\lambda^2+\lambda_c^2)k^2]^{1/2}(1+\nu^2\lambda^2k^2)},$$

$$g_3(k) = \frac{\lambda}{[1+\lambda^2(1+\nu^2)k^2]^{1/2}(1+\nu^2\lambda^2k^2)}.$$

The interaction energy of the chain per unit area E_{TV}^i can be represented as

$$E_{TV}^i = \frac{1}{2a}\sum_{n\neq 0}\int \frac{dk}{2\pi}U_i(k)\exp(ikna) = \frac{1}{2a^2}\sum_{m=-\infty}^{\infty} U_i(k_m) - \frac{1}{2a}\int\frac{dk}{2\pi}U_i(k)$$

with $k_m = 2\pi m/a$, or

$$E_{TV}^i = \sum_{j=1}^{3} E_{TV,j}^i$$

with

$$E_{TV,j}^i = \frac{\pi\varepsilon_0}{a^2}\sum_{m=-\infty}^{\infty}\left[g_j(k_m) - \int_{-\pi/a}^{\pi/a}\frac{adk}{2\pi}g_j(k_m+k)\right].$$

In the limit $a \ll 2\pi\sqrt{\nu^2\lambda^2+\lambda_c^2}$ the first term, $j=1$, can be evaluated as

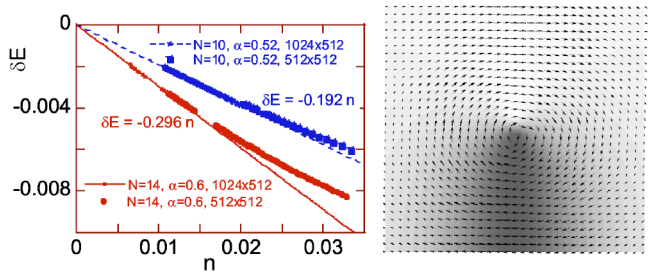

FIG. 12. *Left panel* shows plot of the pancake part of the chain energy per unit area in units ε_0/λ_J, δE, vs pancake density n at very small n. Slope of this energy at $n\to 0$ determines the energy of an isolated kink and the numerical constant C_{kv}. Calculations were made for two sets of parameters, $(N=10, \alpha=0.52)$ and $(N=14, \alpha=0.6)$, and for two system sizes for each set. *Right picture* illustrates the numerically calculated kink structure. Arrows show in-plane currents and gray level plot codes distribution of the cosine of phase difference between the neighboring layers (dark area below corresponds to the Josephson vortex.)

$$E_{TV,1}^i \approx \frac{\varepsilon_0}{a}\left\{\frac{\pi(\nu^2\lambda^2+\lambda_c^2)}{\lambda_c a} - \frac{\sqrt{\nu^2+\gamma^2}}{\gamma} \times\left[\ln\left(\frac{4\pi\sqrt{\nu^2\lambda^2+\lambda_c^2}}{a}\right) - \gamma_E\right]\right\}.$$

Using integral

$$\int_0^\infty \frac{dk}{\sqrt{1+a^2k^2}(1+b^2k^2)} \underset{a>b}{=} \frac{1}{\sqrt{a^2-b^2}}\ln\frac{\sqrt{a^2-b^2}+a}{b},$$

the other two terms are calculated in the limit $c \ll 2\pi\lambda$ as

$$E_{TV,2}^i + E_{TV,3}^i \approx \frac{\varepsilon_0}{a}\left[-\frac{\pi\lambda_c}{a} + \frac{\pi\lambda}{a} + \ln\frac{\gamma+\sqrt{\nu^2+\gamma^2}}{1+\sqrt{1+\nu^2}} - \zeta(3)\left(\frac{c}{2\pi\lambda}\right)^2\left(\frac{\gamma}{\sqrt{\nu^2+\gamma^2}} - \frac{1}{\sqrt{1+\nu^2}}\right)\right].$$

The last term is small and will be dropped in further calculations. Collecting terms, we finally obtain for the total interaction energy (27).

APPENDIX C: ENERGY OF ISOLATED KINK

To find the energy of an isolated kink, we calculated energy of tilted lines in the regime when kink separation $L = a/N$ significantly exceeds the Josephson length. Numerically, this is a challenging task because the kink interaction energy decays slowly with increasing L meaning that one has to go to very large values of a. To maintain sufficient accuracy, one has to use large number of grid points in x direction. As follows from Eq. (32), the pancake part of energy vanishes linearly at small kink concentrations n. In reduced units, we define this energy as $\delta\tilde{E} = (\lambda_J/\varepsilon_0)(E_{TV} - E_{PV}^s - E_{JV})$ and from Eq. (32) we have

$$\delta\tilde{E} \approx n\left(\ln\frac{1}{\alpha} + C_{kv}\right).$$

Plots of this energy are shown in Fig. 12 for two sets of parameters, $(N=10, \alpha=0.52)$ and $(N=14, \alpha=0.6)$. From linear fits at small n we obtain estimates $C_{kv} \approx -0.192 - \ln(1/0.52) \approx 0.846$ for the first set and $C_{kv} \approx -0.296 - \ln(1/0.6) \approx 0.807$ for the second set. If we use the last constant, corresponding to the larger system size, we obtain the estimate $C_k \approx -0.31$ for the constant in the kink energy within Ginzburg-Landau theory (24). This is somewhat smaller than the value -0.17 reported in Ref. 6. The difference is most probably due to finite-size effects.

[1] A. I. Buzdin and D. Feinberg, J. Phys. (Paris) **51**, 1971 (1990); S. N. Artemenko and A. N. Kruglov, Phys. Lett. A **143**, 485 (1990).

[2] J. R. Clem, Phys. Rev. B **43**, 7837 (1991).

[3] B. I. Ivlev, Yu. N. Ovchinnikov, and V. L. Pokrovsky, Mod. Phys. Lett. B **5**, 73 (1991).

[4] L. N. Bulaevskii, M. Ledvij, and V. G. Kogan, Phys. Rev. B **46**, 366 (1992).

[5] D. Feinberg and A. M. Ettouhami, Int. J. Mod. Phys. B **7**, 2085 (1993).

[6] A. E. Koshelev, Phys. Rev. B **48**, 1180 (1993).

[7] A. I. Buzdin and A. Yu. Simonov, JETP Lett. **51**, 191 (1990); A. M. Grishin, A. Y. Martynovich, and S. V. Yampolskii, Sov. Phys. JETP **70**, 1089 (1990); B. I. Ivlev and N. B. Kopnin, Phys. Rev. B **44**, 2747 (1991).

[8] A. E. Koshelev, Phys. Rev. Lett. **83**, 187 (1999).

[9] C. A. Bolle, P. L. Gammel, D. G. Grier, C. A. Murray, D. J. Bishop, D. B. Mitzi, and A. Kapitulnik, Phys. Rev. Lett. **66**, 112 (1991).

[10] I. V. Grigorieva, J. W. Steeds, G. Balakrishnan, and D. M. Paul, Phys. Rev. B **51**, 3765 (1995).

[11] D. A. Huse, Phys. Rev. B **46**, 8621 (1992).

[12] L. L. Daemen, L. J. Campbell, A. Yu. Simonov, and V. G. Kogan, Phys. Rev. Lett. **70**, 2948 (1993); A. Sudbø, E. H. Brandt, and D. A. Huse, *ibid.* **71**, 1451 (1993); E. Sardella, Physica C **257**, 231 (1997).

[13] A. Buzdin and I. Baladié, Phys. Rev. Lett. **88**, 147002 (2002).

[14] A. Grigorenko, S. Bending, T. Tamegai, S. Ooi, and M. Henini, Nature (London) **414**, 728 (2001).

[15] M. J. W. Dodgson, Phys. Rev. B **66**, 014509 (2002).

[16] T. Matsuda, O. Kamimura, H. Kasai, K. Harada, T. Yoshida, T. Akashi, A. Tonomura, Y. Nakayama, J. Shimoyama, K. Kishio, T. Hanaguri, and K. Kitazawa, Science **294**, 2136 (2001).

[17] A. Sudbø and E. H. Brandt, Phys. Rev. B **43**, 10482 (1991).

[18] J. R. Clem and M. W. Coffey, Phys. Rev. B **42**, 6209 (1990); J. R. Clem, M. W. Coffey, and Z. Hao, *ibid.* **44**, 2732 (1991).

[19] A. E. Koshelev, Phys. Rev. B **68**, 094520 (2003).

[20] M. J. W. Dodgson and A. E. Koshelev (unpublished).

[21] M. J. W. Dodgson, Physica C **369**, 182 (2002).

[22] M. Tokunaga, T. Tamegai, Y. Fasano, and F. de la Cruz, Phys. Rev. B **67**, 134501 (2002).

[23] The condition $\nu > N\gamma/2\pi$ means that the separation between kinks L exceeds $c\gamma/2\pi$. In this region the kink interaction energy is strongest for the kinks in the same x-z plane. This planar array of kinks has been called "kink wall" in Ref. 6. Interaction between the neighboring kink walls decays exponentially at large L.

[24] M. Benkraouda and J. R. Clem, Phys. Rev. B **53**, 438 (1996).

[25] A. M. Thompson and M. A. Moore, Phys. Rev. B **55**, 3856 (1997).

[26] See EPAPS Document No. E-PRBMDO-71-031513 for the evolution of the chain structure with decreasing the pancake separation for $N=16$ and $\alpha=0.6$. This document can be reached via a direct link in the online article's HTML reference section or via the EPAPS homepage (http://www.aip.org/pubservs/epaps.html).

[27] R. A. Klemm and J. R. Clem, Phys. Rev. B **21**, 1868 (1980).

[28] W. A. M. Morgado, M. M. Doria, and G. Carneiro, Physica C **349**, 196 (2001).